Observations of nearshore infragravity waves: Seaward and shoreward propagating components

A. Sheremet,[1] R. T. Guza,[2] S. Elgar,[3] and T. H. C. Herbers[4]

Received 14 May 2001; revised 5 December 2001; accepted 20 December 2001; published 6 August 2002.

[1] The variation of seaward and shoreward infragravity energy fluxes across the shoaling and surf zones of a gently sloping sandy beach is estimated from field observations and related to forcing by groups of sea and swell, dissipation, and shoreline reflection. Data from collocated pressure and velocity sensors deployed between 1 and 6 m water depth are combined, using the assumption of cross-shore propagation, to decompose the infragravity wave field into shoreward and seaward propagating components. Seaward of the surf zone, shoreward propagating infragravity waves are amplified by nonlinear interactions with groups of sea and swell, and the shoreward infragravity energy flux increases in the onshore direction. In the surf zone, nonlinear phase coupling between infragravity waves and groups of sea and swell decreases, as does the shoreward infragravity energy flux, consistent with the cessation of nonlinear forcing and the increased importance of infragravity wave dissipation. Seaward propagating infragravity waves are not phase coupled to incident wave groups, and their energy levels suggest strong infragravity wave reflection near the shoreline. The cross-shore variation of the seaward energy flux is weaker than that of the shoreward flux, resulting in cross-shore variation of the squared infragravity reflection coefficient (ratio of seaward to shoreward energy flux) between about 0.4 and 1.5. *INDEX TERMS:* 4546 Oceanography: Physical: Nearshore processes; 4560 Oceanography: Physical: Surface waves and tides (1255); 4594 Oceanography: Physical: Instruments and techniques; *KEYWORDS:* infragravity waves, energy flux, surf zone, nonlinear phase coupling, shoreline reflection, cross-shore evolution

1. Introduction

[2] Over a distance of just a few wavelengths on a moderately sloped beach, shoreward propagating sea and swell (periods of roughly 4–20 s) steepen, pitch forward, break, and form dissipative bores. This evolution is accompanied by the generation of gravity waves with periods of a few minutes (infragravity waves). Here field observations are used to estimate the variation of seaward and shoreward infragravity energy fluxes across the shoaling and surf zones.

[3] Previous field observations have shown that standing waves can be a dominant component of the nearshore infragravity wave field [e.g., *Suhayda*, 1974; *Huntley*, 1976; *Huntley et al.*, 1981; *Oltman-Shay and Howd*, 1993]. Standing infragravity waves are consistent with relatively weak forcing and damping and strong shoreline reflection. However, there also is evidence that a substantial progressive infragravity component can result from nonlinear forcing of shoreward propagating infragravity waves by groups of sea and swell [e.g., *Munk*, 1949; *Longuet-Higgins and Stewart*, 1962; *Meadows et al.*, 1982; *Elgar and Guza*, 1985; *List*, 1992; *Herbers et al.*, 1994]. Nonlinearly forced shoreward propagating and free seaward propagating (resulting from shoreline reflection) infragravity waves are expected to have different cross-shore amplitude variations, leading to partially standing waves. Observations in 13 m water depth, 2 km offshore of Duck, North Carolina (the site of the observations presented here), show that the net (integrated over the infragravity frequency band) energy flux can be directed either seaward or shoreward and that the ratio of seaward to shoreward fluxes (hereinafter the bulk infragravity reflection coefficient R^2) deviates substantially from 1, with values usually between 0.5 and 4.0 [*Elgar et al.*, 1994; *Herbers et al.*, 1995b]. Reflection coefficients <1 (>1) imply an energy sink (source) between the shoreline and 13 m depth observation sites. Three R^2 regimes were identified. With low sea-swell energy the infragravity wave field was dominated by arrivals from remote sources that were either partially dissipated or scattered into trapped waves shoreward of 13 m depth, and $R^2 < 1$. With moderate sea-swell energy, infragravity energy generated onshore of 13 m depth and radiated seaward exceeded dissipation and trapping losses, and $R^2 > 1$. With the most energetic sea and swell waves the

[1]Coastal Studies Institute and Department of Oceanography and Coastal Sciences, Louisiana State University, Baton Rouge, Louisiana, USA.
[2]Integrative Oceanography Division, Scripps Institution of Oceanography, La Jolla, California, USA.
[3]Woods Hole Oceanographic Institution, Woods Hole, Massachusetts, USA.
[4]Department of Oceanography, Naval Postgraduate School, Monterey, California, USA.

0148-0227/02/2001JC000970$09.00

13 m depth observations were near the surf zone where dissipation might be important, and $R^2 < 1$. Nonlinear phase coupling of infragravity waves to groups of sea and swell seaward of the surf zone (depths between about 8 and 200 m) has been investigated with observations in the Atlantic and Pacific Oceans [*Herbers et al.*, 1994, 1995b]. The observed levels of phase coupling, estimated with bispectral analysis, agreed well with the theory for second-order bound waves driven by quadratic, nonresonant, sea-swell interactions [*Hasselmann*, 1962], and both the bound wave energy levels and the ratio of bound to total (free plus bound) infragravity energy increased with increasing sea-swell energy and decreasing depth. Similar increases in nonlinear phase coupling were observed in pressure measurements seaward of the surf zone (in 3–6 m depth) [*Ruessink*, 1998]. However, the coupling decreased to approximately zero when the offshore sea-swell energy was so large that the observations were within the surf zone.

[4] Here a more detailed analysis of the transformation of infragravity waves through the shoaling and surf zones is presented using extensive new observations. Collocated current meters and pressure sensors deployed in 1–6 m depth (described in section 2) are used to decompose the infragravity wave field into shoreward and seaward propagating components. Errors introduced by neglecting the directionality of the infragravity wave field are shown to be small in Appendix A. The spatial variation of infragravity energy fluxes is related to forcing by groups of sea and swell, dissipation, and shoreline reflection in section 3. The directionality of infragravity waves is discussed briefly in section 4. A more detailed analysis is presented by A. Sheremet et al. (manuscript in preparation, 2002). Results are summarized in section 5.

2. Field Experiment and Analysis

[5] Observations were obtained from August to December 1997 during the Sandyduck experiment conducted on a sandy beach near Duck, North Carolina. A two-dimensional array of electromagnetic current meters, downward looking sonar altimeters, and pressure sensors was deployed in 1–6 m depth, 50–350 m from the shoreline (Figure 1). Bathymetric surveys obtained a few times a week with an amphibious vehicle were supplemented with nearly continuous altimeter observations. There was a 50 cm high sandbar crest in about 3.5 m mean water depth (cross-shore location x = 320 m) and a transient sandbar in about 1 m depth (x = 160 m) (Figure 1). Alongshore variability of the bathymetry usually was weak over the instrumented area, except near the shoreline. *Feddersen et al.* [2000] and *Elgar et al.* [2001] give additional details and describe conditions during the experiment.

[6] To investigate cross-shore energy fluxes, surface elevation time series of shoreward and seaward propagating infragravity waves (η^+ and η^-, respectively) are constructed from collocated pressure p and cross-shore velocity u time series using the assumptions of shallow water and cross-shore propagation [*Guza et al.*, 1984; *Elgar and Guza*, 1985; *List*, 1992],

$$\eta^{\pm} = \frac{1}{2}\left(p \pm u\sqrt{h/g}\right), \tag{1}$$

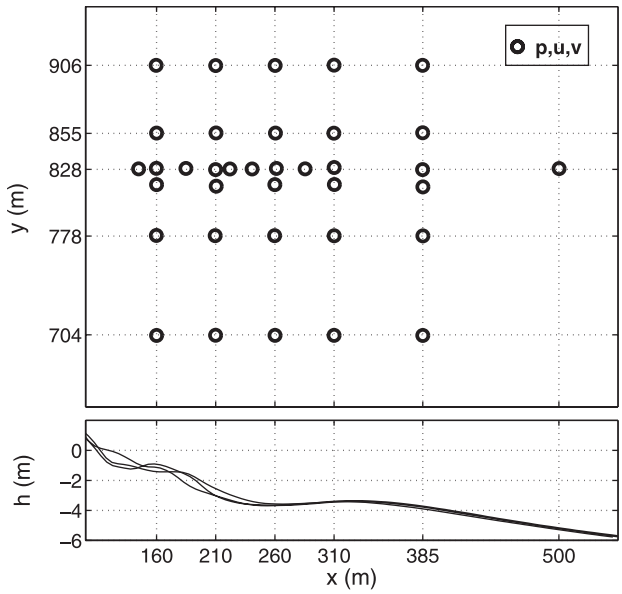

Figure 1. (top) Plan view of instrument array. Circles are collocated pressure (p) and horizontal velocity (u and v) sensors. Current meters usually were positioned between 50 and 100 cm above the seafloor. The Field Research Facility coordinate frame is used, with x and y the cross-shore and alongshore directions, respectively. Additional pressure gages in 8 m depth (x = 800 m) are not shown. (bottom) Alongshore-averaged seafloor elevation relative to mean sea level versus x (collected during August, September, and November).

where h is the depth and g is the gravity. The corresponding energy $\mathcal{E}$ and cross-shore energy fluxes $\mathcal{F}$ of shoreward and seaward propagating waves (superscripts ±, respectively) at frequency f and location x are

$$\mathcal{E}^{\pm}(f,x) = \frac{1}{4}\left[Co_{pp}(f,x) + (h/g)Co_{uu}(f,x). \pm \left(2\sqrt{h/g}\right)Co_{pu}(f,x)\right], \tag{2}$$

$$\mathcal{F}^{\pm}(f,x) = \mathcal{E}^{\pm}(f,x)\sqrt{gh}, \tag{3}$$

where Co_{pu} is the $p - u$ cospectrum and Co_{pp} and Co_{uu} are p and u autospectra, respectively. Unlike the individual shoreward and seaward fluxes (equation (3)), the net cross-shore flux ($\mathcal{F}^+ - \mathcal{F}^- = hCo_{pu}$) does not require the assumption of near shore normal propagation [*Stoker*, 1947].

[7] The pressure and current meter data, sampled at 2 Hz and processed in 3 hour segments, were quadratically detrended and then divided into 448 s demeaned ensembles with 50% overlap. After tapering each ensemble with a Hanning window, cross spectra and spectra with about 48 degrees of freedom and frequency resolutions of 0.002 Hz were calculated. Energy flux densities (equation (3)) were integrated over the infragravity frequency band (0.004–0.05 Hz) to estimate bulk infragravity fluxes $F^{\pm}$ and bulk reflection coefficients R^2:

$$F^{\pm}(x) = \int_{0.004\text{Hz}}^{0.05\text{Hz}} \mathcal{F}^{\pm}(f,x)df,\ R^2(x) = F^-(x)/F^+(x)\ . \tag{4}$$

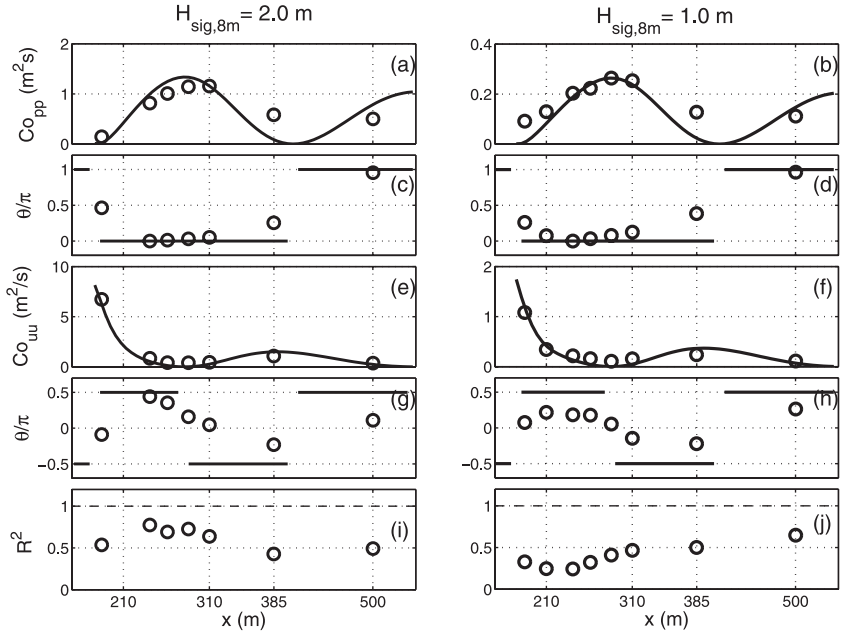

Figure 2. (a) and (b) Pressure spectral density Co_{pp}; (c) and (d) normalized phase difference θ/π between pressure at $x = 240$ m and pressure at other cross-shore locations; (e) and (f) cross-shore velocity spectral density Co_{uu}; (g) and (h) normalized phase difference θ/π between collocated pressure and cross-shore velocity; and (i) and (j) infragravity reflection coefficient R^2 versus cross-shore location x: (left) 7 November 1997, 0700–1000 EST, offshore significant sea-swell wave height $H_{\mathrm{sig,8m}} = 2.0$ m. (right) 10 September 1997, 0100–0400 EST, $H_{\mathrm{sig,8m}} = 1.0$ m. The frequency is 0.014 Hz. The circles are observations, and the solid curves are solutions of the linear shallow-water equations for a normally incident cross-shore standing wave ($R^2 = 1$) on the measured bathymetry. The predicted Co_{pp} and Co_{uu} are normalized with the maximum observed value.

Bulk infragravity energies, fluxes, and reflection coefficients were obtained from each collocated $p - u$ sensor pair. Estimates from the same alongshore array (Figure 1) were averaged. Errors in the bulk fluxes and R^2 owing to the assumption of normal incidence are estimated to be <20% (Appendix A). To eliminate observations with significant nongravity motions (e.g., shear waves), 3 hour runs with a mean alongshore velocity >50 cm s^{-1} at any current meter were excluded. Frequency–alongshore wave number spectra (T. J. Noyes, personal communication, 2000) confirm that nongravity wave motions contribute generally <20% of the infragravity velocity variance in the 680 runs retained in this study. Linear finite depth theory was applied to pressure data in 8 m depth to estimate $E_{ss,8\mathrm{m}}$, the sea-swell energy integrated over the frequency band 0.05–0.24 Hz. Significant wave heights in 8 m depth, $H_{\mathrm{sig,8m}} = 4E^{1/2}_{ss,8\mathrm{m}}$, in the retained 3 hour runs ranged from 0.2 to 2.7 m.

[8] Quadratic difference-frequency interactions between sea-swell components with slightly different frequencies (f and $f + \Delta f$) are always nonresonant in intermediate and deep (for the sea and swell waves) water depths and, theoretically, result in a bound infragravity wave of frequency Δf that does not satisfy the linear dispersion relation. In this nonresonant case the doubly integrated, normalized bispectrum (b_{ii} in equation (9) of *Herbers et al.* [1994] and μ here) is proportional to the fraction of the total infragravity wave energy contained in bound components. In contrast, when the water depth is shallow for the sea and swell, near-resonant quadratic difference-frequency interactions can result in gradual (over several wavelengths) alteration of the phase and energy of free infragravity waves. In this case the real and imaginary parts of the bispectrum are related to the rate of nonlinear phase change (wave number shift) and nonlinear energy exchange, respectively [*Herbers and Burton*, 1997; *Herbers et al.*, 2002]. Therefore, in the shallow depths considered here, μ (incorporating both real and imaginary parts of the bispectrum) is interpreted qualitatively as a nondimensional measure of the strength of near-resonant forcing of free infragravity waves by quadratic interactions with sea and swell.

[9] Calculating μ from observed pressure or velocity time series mixes information about seaward and shoreward propagating infragravity waves. Following *Elgar and Guza* [1985], nonlinear coupling also was estimated from time series of pressure fluctuations containing only shoreward or only seaward propagating infragravity waves (μ^+ and μ^-, calculated using η^+ and η^- (equation (1)), respectively). An error in accounting for the effect of time domain windowing in previously reported bispectral integrals [*Herbers et al.* 1994, 1995a; *Ruessink*, 1998] is corrected below, resulting in μ, μ^+, and μ^- values that are a factor of 0.58 lower than uncorrected values.

3. Results

[10] Similar to previous observations [e.g., *Suhayda*, 1974], at a fixed infragravity frequency the observed cross-shore variation of spectral levels of pressure (Figures 2a and 2b) and cross-shore velocity (Figures 2e and 2f) have

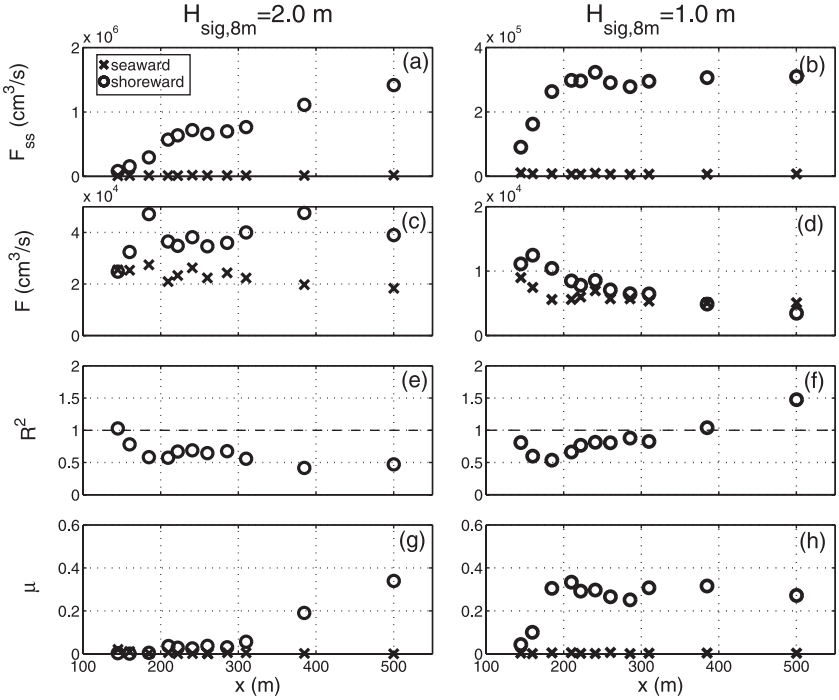

Figure 3. (a) and (b) Bulk seaward and shoreward sea-swell energy fluxes; (c) and (d) bulk seaward and shoreward infragravity energy fluxes; (e) and (f) bulk infragravity reflection coefficient R^2; and (g) and (h) measures of nonlinear phase coupling $\mu^{\pm}$ versus cross-shore location x:(left) 7 November 1997, 0700–1000 EST, $H_{sig,8m}$ = 2.0 m and (right) 10 September 1997, 0100–0400 EST, $H_{sig,8m}$ = 1.0 m. The μ^{+} biphases, not shown, are close to 180°, as observed by *Ruessink* [1998]. Circles and crosses correspond to shoreward and seaward infragravity wave propagation, respectively. Note the different vertical scales for fluxes in the left and right panels.

minima and maxima close to the theoretical locations of standing wave nodes and antinodes.

[11] Note that the observed u spectral maxima and p spectral minima occur at the same location (e.g., x = 185 m), in contrast to a progressive wave field where the spatial variations of u and p spectral levels are similar and do not have a structure with nodes and antinodes. The observed phase differences between spatially separated p time series (Figures 2c and 2d) and between collocated p and u time series (Figures 2g and 2h) also suggest substantial shoreline reflection. With a progressive wave field on a gently sloping bottom the phase difference between spatially separated time series increases approximately linearly with increasing separation along the propagation direction, and the phase between collocated p and u is zero. At the representative infragravity frequency (0.014 Hz) shown in Figure 2, strong reflection is confirmed by the $R^2(f)$ estimates (based on collocated pressure and cross-shore velocity observations equations (2) and (3)) in the range 0.2–0.8 (Figures 2i and 2j). As discussed by A. Sheremet et al. (manuscript in preparation, 2002), similar reflection coefficient estimates are obtained when spatially separated sensors are included in the analysis. Individual frequency bands are not considered further here.

[12] In both wide ($H_{sig,8m}$ = 2.0 m) and narrow ($H_{sig,8m}$ = 1.0 m) surf zone cases, infragravity wave reflection is significant (Figures 3e and 3f), whereas sea-swell reflection is weak (Figures 3a and 3b). The bulk shoreward infragravity flux F^{+} increases shoreward in the region where μ^{+} is large (roughly $x \geq$ 385 m in Figures 3c and 3g and $x \geq$ 175 m in Figures 3d and 3h). Within the surf zone, μ^{+} decreases to negligible values, and the growth of F^{+} ceases (with the exception of one observation at x = 175 m in Figure 3c). Seaward propagating infragravity waves are not coupled to groups of sea and swell (μ^{-} is small everywhere; Figures 3g and 3h). The bulk reflection coefficient R^2 (equation (4)) decreases from values as large as 1.5 far seaward of the surf zone (Figure 3f) to between about 0.5 and 1.0 within the surf zone (Figures 3e and 3f). At the location nearest the shoreline, $R^2 \approx 1$. These trends are consistent with the hypotheses [e.g., *Longuet-Higgins and Stewart*, 1962] that F^{+} increases in the shoaling region owing to nonlinear forcing by sea-swell groups, that sea-swell breaking reduces the nonlinear forcing, and that shoreward propagating infragravity waves are reflected strongly at the shoreline.

[13] At the most offshore p–u location (x = 500 m) the seaward F^{-} and shoreward F^{+} fluxes both increase with increasing $E_{ss,8m}$ (Figures 4a and 4c). For all $E_{ss,8m}$, F^{-} at x = 500 m (5–6 m depth) and x = 210 m (2–3 m depth) are approximately equal (their ratio is about 1.2; Figure 4b). In contrast, the ratio of F^{+} at x = 210 m to F^{+} at x = 500 m is as large as 3 with moderate $E_{ss,8m}$ and is <1 with the largest $E_{ss,8m}$ (Figure 4d).

[14] At the deepest (5–6 m depth) location the dependence of the bulk reflection coefficient R^2 on $E_{ss,8m}$ (Figure 5a) is similar to that observed in 13 m depth [*Herbers et al.*, 1995b, Figure 5]. For moderate values of

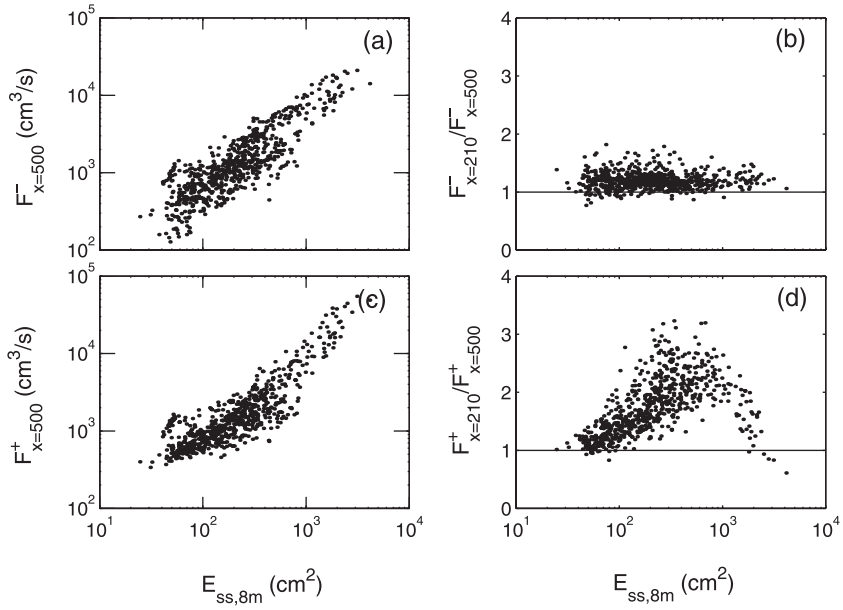

Figure 4. (a) Bulk seaward infragravity energy flux F^- at x = 500 m; (b) bulk ratio of F^- at x = 210 to F^- at x = 500 m; (c) bulk shoreward infragravity energy flux F^+ at x = 500 m; and (d) bulk ratio of F^+ at x = 210 to F^+ at x = 500 m versus sea-swell energy in 8 m depth, $E_{ss,8m}$.

$E_{ss,8m}$, $R^2 > 1$, whereas for the largest and smallest $E_{ss,8m}$, $R^2 < 1$. However, the maximum R^2 values here are about 1.5, lower than those observed (as high as 4.0) in 13 m depth. Closer to shore (x = 210 m), $R^2 < 1$ for all $E_{ss,8m}$ (Figure 5b). Although values are scattered, at both locations the mean R^2 decreases with large and increasing $E_{ss,8m}$. At both locations the nonlinear coupling μ^+ increases as $E_{ss,8m}$ increases from the lowest levels, reaches a maximum at intermediate $E_{ss,8m}$ values, and then decreases with further increases in $E_{ss,8m}$ (Figures 5c and 5d).

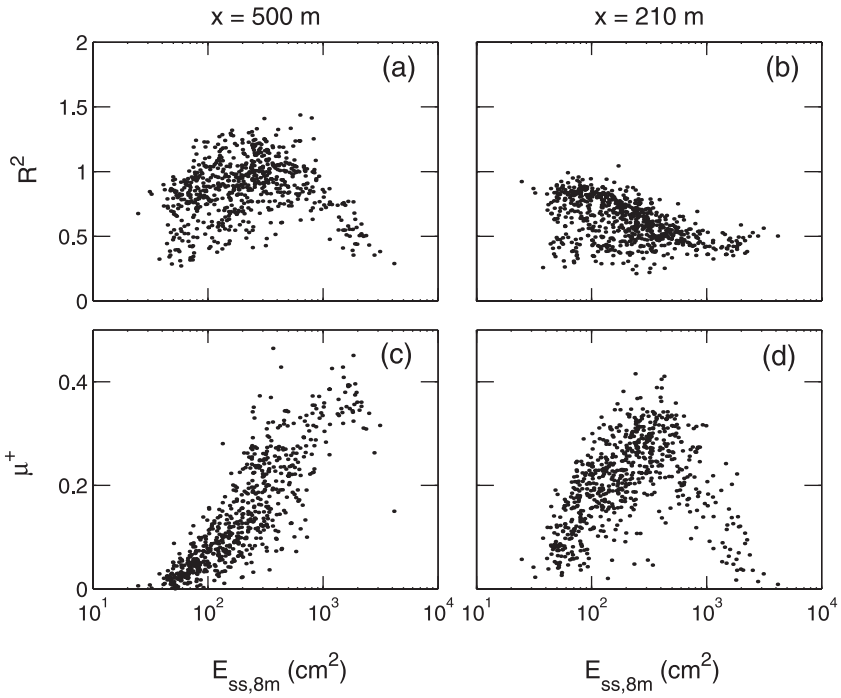

Figure 5. (a) and (b) Bulk infragravity reflection coefficient R^2 and (c) and (d) bulk nonlinear phase-coupling μ^+ versus sea-swell energy in 8 m depth $E_{ss,8m}$ at cross-shore locations (left) x = 500 and (right) x = 210 m.

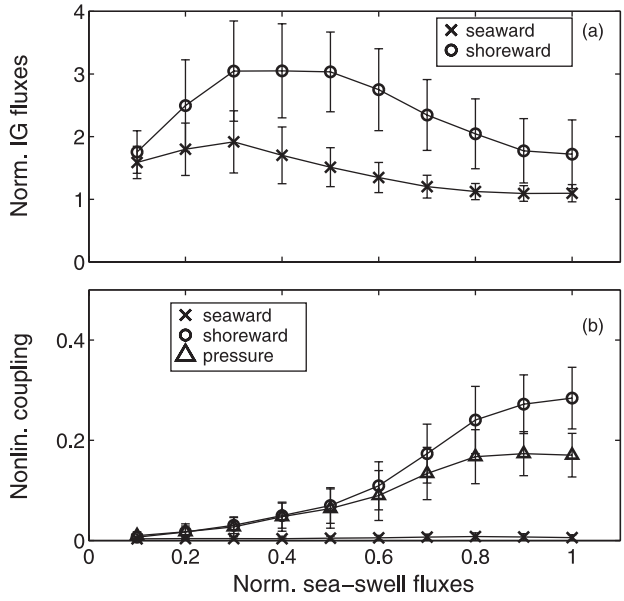

Figure 6. (a) Average values of bulk shoreward F^+ (circles) and seaward F^- (crosses) infragravity energy fluxes normalized by $F_{x=500}$, the seaward infragravity flux at x = 500 m, and (b) bulk nonlinear phase coupling to sea-swell groups of the total (μ, triangles), shoreward propagating (μ^+, circles), and seaward propagating (μ^-, crosses) infragravity wave fields versus the shoreward sea-swell energy flux F^+_{ss} normalized by the sea-swell flux in 8 m depth $F^+_{ss,8m}$. The vertical bars indicate ±1 standard deviation about the mean. When offshore sea and swell energy are low, the dominant infragravity waves often are arrivals from remote sources [*Herbers et al.*, 1995b]. To focus on locally generated infragravity waves, 385 3 hour runs with $E_{ss,8m} > 400$ cm^2 are used.

[15] On the basis of similar variations of observed μ with E_{ss}, *Ruessink* [1998] suggested that the intense wave breaking in the surf zone reduces the forcing of infragravity waves. The dependence of the normalized infragravity fluxes and nonlinear coupling on the reduction of sea-swell energy flux in the surf zone (F^+_{ss} normalized by the flux in 8 m depth, $F^+_{ss,8m}$) is shown in Figure 6. Values of the normalized sea-swell flux $F^+_{ss}/F^+_{ss,8m}$ close to 1 correspond to observations seaward of the surf zone, and lower values are progressively farther within the surf zone. The normalized shoreward infragravity flux $F^+/F^-_{x=500m}$ increases as $F^+_{ss}/F^+_{ss,8m}$ decreases from 1, reaches a maximum for $F^+_{ss}/F^+_{ss,8m} \approx 0.5$, and then decreases in the inner surf zone (Figure 6a). This decrease suggests significant damping of infragravity waves in the surf zone. Similar to the nonlinear coupling of the total infragravity field μ to groups of sea and swell [*Ruessink*, 1998], the coupling of shoreward propagating infragravity waves μ^+ is reduced greatly in the surf zone (Figure 6b), consistent with the cessation of nonlinear forcing.

[16] Although the dependence of infragravity wave properties on the normalized sea-swell flux $F^+_{ss}/F^+_{ss,8m}$ demonstrates the important role of sea-swell breaking, all observations seaward of the surf zone are collapsed into $F^+_{ss}/F^+_{ss,8m} \approx 1$. Consequently, the variation of infragravity fluxes observed in the shoaling region (i.e., $x \geq 175$ m in Figure 3d) is obscured. To include this spatial variation, infragravity wave properties are shown (Figure 7) as functions of the normalized cross-shore position x/x_{50}, where x_{50} is the location where F^+_{ss} is 50% of $F^+_{ss,8m}$ and the shoreward infragravity flux is maximum (Figure 7a). $F^+/F^-_{x=500m}$ increases in the shoaling region, attains a maximum at about $x/x_{50} = 1.0$, and then decreases (Figure 7a). The coupling μ^+ is nearly constant through the shoaling region, then starting at the outer edge of the surf zone ($x/x_{50} \approx 2$) decreases sharply to negligible values in the inner surf zone ($x/x_{50} < 1$) (Figure 7b). Seaward propagating infragravity waves are not phase coupled to sea-swell groups (μ^- always is small; Figure 6b), and the energy flux of the unforced seaward propagating waves F^- is less spatially variable than the flux F^+ of the nonlinearly forced shoreward propagating waves (Figure 7a). Dissipation and refractive trapping, discussed by A. Sheremet et al. (manuscript in preparation, 2002), both contribute to the decrease in F^- with increasing offshore distance from the shoreline.

[17] The dependence of R^2 estimates on x/x_{50} is shown in Figure 8, including additional estimates farther from shore based on array measurements in 8 m depth. Although the analysis methods are different, R^2 estimates based on nearshore collocated p, u observations and offshore array measurements (analyzed without the assumption of normal incidence [*Herbers et al.*, 1995b]) overlap smoothly at intermediate x/x_{50} values (Figure 8). Far offshore of the surf zone (largest x/x_{50}), $F^- > F^+$ and the bulk reflection coefficient R^2 approaches 1.6 (Figure 8).

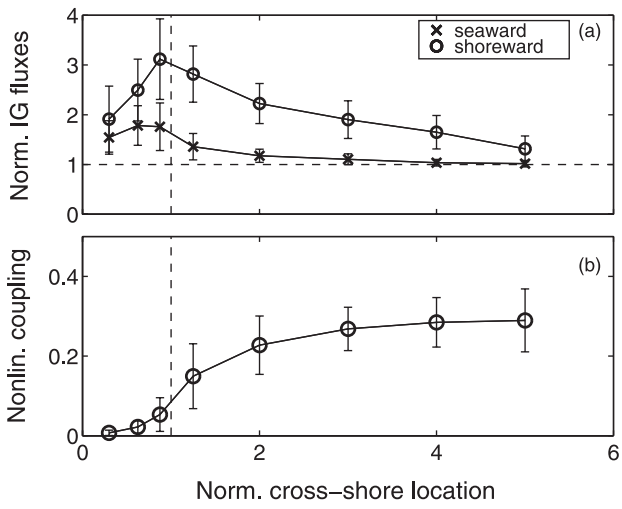

Figure 7. (a) Average values of bulk shoreward F^+ (circles) and seaward F^- (crosses) infragravity energy fluxes normalized by $F^-_{x=500}$, the seaward infragravity flux at x = 500 m, and (b) bulk nonlinear phase coupling to sea-swell groups of shoreward propagating infragravity waves (μ^+, circles) versus x/x_{50}, where x_{50} is the cross-shore location where the shoreward sea-swell flux is reduced to 50% of the flux in 8 m depth. The dashed vertical line indicates $x/x_{50} = 1$. The vertical bars indicate ±1 standard deviation about the mean. To focus on locally generated infragravity waves, 385 3 hour runs with $E_{ss,8m} > 400$ cm^2 are used.

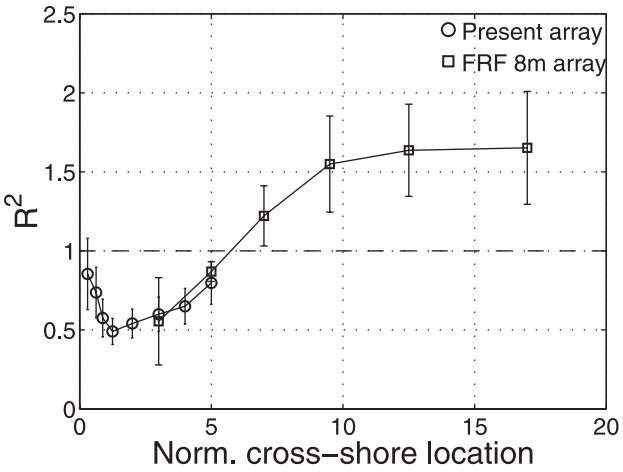

Figure 8. Bulk infragravity reflection coefficient R^2 versus normalized cross-shore location x/x_{50}. Circles are estimates based on collocated p - u sensors (equation (1), depths <6 m), and squares are based on pressure array observations in 8 m depth. The 385 3 hour runs with $E_{ss,8m} > 400$ cm^2 are used.

During shoaling, F^+ increases, but F^- remains relatively constant (Figure 7a), and R^2 decreases to a minimum of about 0.5 near $x/x_{50} = 1$. In the inner surf zone ($x/x_{50} < 1$) where F^+ decreases toward shore (presumably owing to dissipation), R^2 increases again to a maximum value of about 0.8 at the shoreline where the infragravity waves are strongly reflected.

[18] Numerical and laboratory studies suggest that infragravity energy also may be generated by fluctuations of surf zone (Figure 7a) width and setup at infragravity periods [*Symonds et al.*, 1982; *Lippmann et al.*, 1997]. Although such generation is not precluded by the results presented here, much of the observed growth in F^+ occurs well seaward of the surf zone and thus offshore of the region where generation by a time-varying breakpoint theoretically occurs.

4. Directionality of Infragravity Waves

[19] The method used here to estimate the shoreward and seaward propagating infragravity wave components is based on the assumption of near shore normal propagation. Although the energy flux and R^2 estimates are not degraded significantly by the infragravity wave obliquity in these data (Appendix A), obliquity could be associated with refractively trapped edge waves. As in previous studies in similar water depths [e.g., *Huntley et al.*, 1981; *Oltman-Shay and Howd*, 1993], frequency and frequency–wave number spectra show deviations from normal incidence. In cases with large mean incident angles the spectral levels of v often are within a factor of 2–3 of the cross-shore velocity u levels (Figure 9a). At infragravity frequencies, frequency–alongshore wave number spectra of p, u, and v (p is shown in Figure 9b) have variance maxima at wave numbers within the edge wave range. On the basis of frequency-alongshore wave number spectra and the qualitative standing wave character of the cross-shore variation of infragravity phases and variance (Figures 2b, 2d, 2f, and 2h), observations similar to these have been interpreted as consistent with edge waves, the normal mode solutions of gravity waves undergoing multiple reflections between the shoreline and an offshore turning point. However, the cross-shore analysis for this run shows a substantial progressive shoreward energy flux (Figure 3f) that suggests that a significant fraction of the energy is lost before waves reach the shoreline. This motivates the consideration of strongly damped edge waves by A. Sheremet et al. (manuscript in preparation, 2002).

5. Conclusions

[20] Observations of pressure and velocity collected in water depths between 1 and 6 m are used to estimate the seaward and shoreward energy fluxes of infragravity waves. Although there is considerable scatter, on average the shoreward infragravity flux increases during shoaling when the nonlinear coupling between shoreward propagating infragravity waves and sea-swell groups is strongest. Within the surf zone, coupling is reduced strongly, and the shoreward flux decreases, consistent with the cessation of forcing and increased dissipation. Reflection is strong at the shoreline. The coupling of seaward propagating infragravity waves to sea-swell groups always is weak. The results support the existing hypothesis that shoreward propagating infragravity waves are amplified in the shoaling zone by nonlinear interactions with sea-swell groups and are strongly reflected near the shoreline. Damping of infragravity waves in the surf zone also appears to be important. The seaward infragravity flux decreases with increasing distance from the shoreline, consistent with both dissipation and refractive trapping, but is less spatially variable than the shoreward flux. As a result of these spatially varying energy fluxes, the bulk infragravity reflection coefficient exceeds 1 far seaward of the surf zone, reaches a minimum of about 0.4 in the outer surf zone, and increases to about 0.8 at the shoreline where infragravity waves are reflected strongly.

Appendix A: Error Estimates for R^2 and $F^{\pm}$

[21] Errors in infragravity energy fluxes and reflection coefficients estimated using collocated observations of pressure p and cross-shore velocity u and the assumption of normal incidence (equations (2) and (3)) are examined using linear WKB theory for shallow-water waves. The cross-shore and the alongshore coordinates are x and y, and the x origin is at the shoreline. Assuming that the depth varies only in the cross-shore direction, $h = h(x)$, the pressure time series can be expressed as a superposition of Fourier modes with different frequencies f and alongshore wave numbers k_y:

$$p(t,x,y) = \int_{\infty}^{\infty} df\ e^{-2\pi i f t} \int_{\infty}^{\infty} P'(f,x,k_y) e^{ik_y y} \frac{dk_y}{2\pi}$$

or, equivalently, incidence angles $\theta(f, x)$:

$$p(t,x,y) = \int_{-\infty}^{\infty} df\, e^{-2\pi i f t} \int_{-\pi}^{\pi} P(f,x,\theta) e^{ik\sin\theta} d\theta, \qquad \text{(A1)}$$

where P is the cross-shore structure of a Fourier mode and $k = k(f, x)$ is the local wave number modulus. Normal

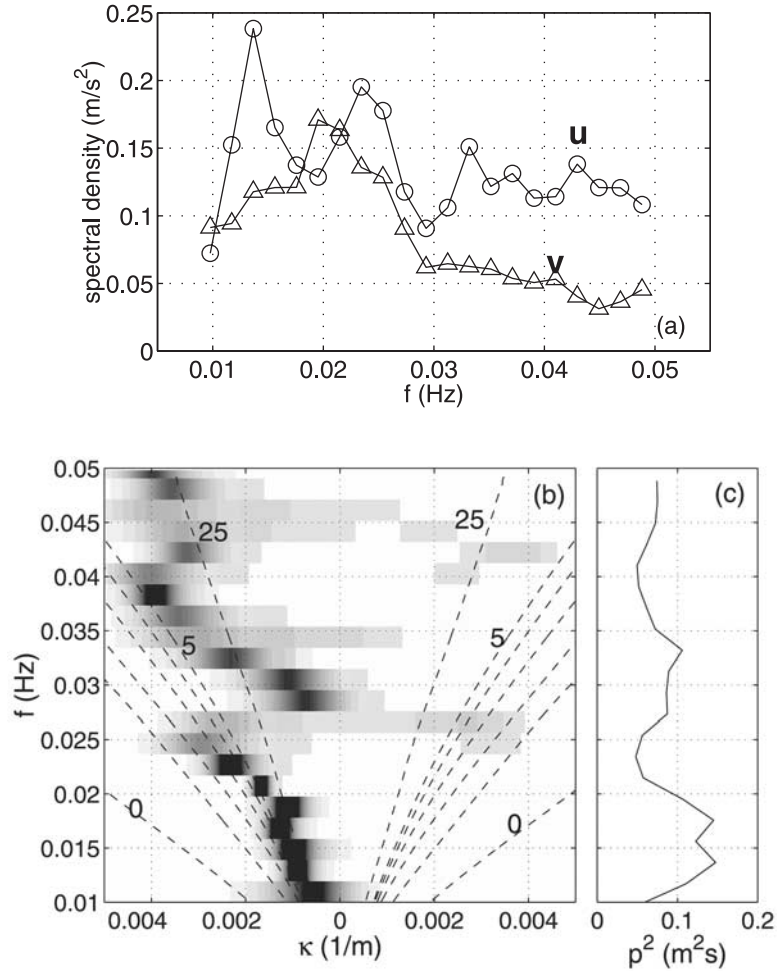

Figure 9. (a) Frequency spectra of infragravity cross-shore u (circles) and alongshore v (triangles) velocities, (b) normalized frequency-cyclic alongshore wave number ($f - \kappa$) spectra of pressure p estimated with the Maximum Entropy Method [*Wu*, 1997], and (c) frequency spectra of pressure at x = 310 m, on 10 September, 0100–0400 EST. The dashed curves in Figure 9b are edge wave dispersion curves for modes 0–5 (approximately the boundary between the leaky and trapped wave domains). The $f - \kappa$ spectra at each f are normalized by the frequency spectra, and darker shades indicate higher spectral levels within each frequency band. Additional results for this run are shown in Figures 2(right) and 3(right).

incidence corresponds to $\theta = 0$. A relation similar to equation (A1) can be written for U, the cross-shore structure of the cross-shore velocity. P and U are assumed to have the form

$$P(f,x,\theta) = \frac{1}{2}\left[A^+ e^{i\phi+i\epsilon_+} + A^- e^{-i\phi+i\epsilon_-}\right],$$
$$U(f,x,\theta) = \frac{1}{2}\sqrt{\frac{g}{h}}\left[A^+ e^{i\phi+i\epsilon_+} - A^- e^{-i\phi+i\epsilon_-}\right]\cos\theta, \quad \text{(A2)}$$

where $A^{\pm} = A^{\pm}(f, x, \theta)$ are the real amplitudes of shoreward (+) and seaward (−) propagating waves, $\epsilon_{\pm}$ is an arbitrary phase, and ϕ is the phase with respect to the shoreline

$$\phi(f,x,\theta) = \int_0^x k_x ds = 2\pi f \int_0^x \frac{\cos\theta(f,s,\Theta)}{\sqrt{gh(s)}} ds, \quad \text{(A3)}$$

where $\Theta = \theta(f, x)$ is the incidence angle at the seaward edge of the integration domain and k_x is the cross-shore wave number, respectively. Shoreward propagating waves are assumed to be partially reflected at the shoreline, with the WKB phases $\epsilon_+ - \epsilon_- = -\pi/2$ determined by matching to exact standing wave solutions [*Herbers et al.*, 1995a]. Using equation (A2), the autospectra and cross-spectra for collocated pressure and cross-shore velocity time series are

$$\mathbf{X}_{pp}(f,x) = \frac{1}{2}\int_{-\pi/2}^{\pi/2}\left[(A^+)^2 + (A^-)^2 + 2A^+A^-\sin(2\phi)\right]d\theta,$$

$$\mathbf{X}_{uu}(f,x) = \frac{1}{2}\int_{-\pi/2}^{\pi/2}\left[(A^+)^2 + (A^-)^2 - 2A^+A^-\sin(2\phi)\right]\cos^2\theta d\theta,$$

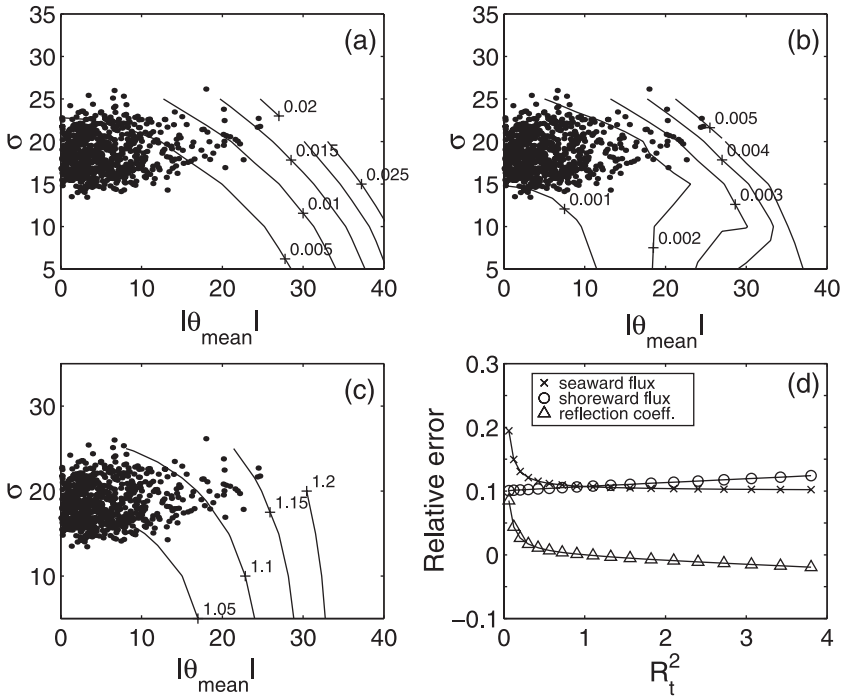

Figure A1. Contours of (a) R_0^2, (b) the magnitude of the maximum value attained by $|\beta|$ over a plane beach with a 0.02 slope, over the depth range 1–6 m, and (c) F_0^+/F_t^+ as functions of the mean direction θ_m and directional spread σ (angular spread function $S(\theta)$ is defined in equation (A14)). Each dot represents the alongshore-averaged bulk infragravity mean direction and directional spread for a single 3 hour run at a given cross-shore location, computed with a method that utilizes both components of horizontal velocity [*Herbers et al.*, 1999]. (d) The relative errors of R^2 and $F^{\pm}$ for $R_0^2 = 0.005$, $|\beta| = 0.0015$, and $F_0^+/F_t^+ = 1.1$ (e.g., the relative error for R^2 is defined as $(R^2 - R_t^2)/R_t^2$) versus the true reflection coefficient R_t^2.

$$\mathbf{X}_{pu}(f,x) = \frac{1}{2}\int_{-\pi/2}^{\pi/2}\left[(A^+)^2 - (A^-)^2 + 2iA^+A^-\cos(2\phi)\right]\cos\theta d\theta \tag{A4}$$

[22] Substituting equation (A4) into equations (2)–(3) yields the estimated energy fluxes at frequency f:

$$\mathcal{F}^{\pm} = \frac{\sqrt{gh}}{8}\int_{-\pi/2}^{\pi/2}\left\{\left[(A^+)^2 + (A^-)^2\right](1+\cos^2\theta) \pm 2\left[(A^+)^2 - (A^-)^2\right]\cos\theta + 2A^+A^-(2\phi)\sin^2\theta\right\}d\theta. \tag{A5}$$

The amplitudes are related to the energy $\mathcal{E}^+$ and angular distribution S of the shoreward propagating modes by

$$\begin{aligned}(A^+)^2 &= 2\mathcal{E}^+(f,x)S(f,\theta),\\ (A^-)^2 &= 2R_t^2\mathcal{E}^+(f,x)S(f,\theta),\\ A^+A^- &= 2R_t\mathcal{E}^+(f,x)S(f,\theta),\end{aligned} \tag{A6}$$

where $\int_{-\pi/2}^{\pi/2} S(f,\theta)\, d\theta = 1$. Specular reflection and a true reflection coefficient R_t that is independent of frequency and direction are assumed for simplicity. With $\mathcal{E}^+$ and S assumed independent of frequency over the infragravity band the frequency-integrated fluxes are

$$F^{\pm} = \sqrt{\frac{gh}{4}}E^+\left\{\int_{-\pi/2}^{\pi/2} d\theta\, S(\theta)\cdot\left[(1+R_t^2)(1+\cos^2\theta) \pm 2(1-R_t^2)\cos\theta\right] + \frac{2}{\Delta_f}\int_{D_f} df\int_{-\pi/2}^{\pi/2} S(\theta)R_t\sin(2\phi)\sin^2\theta d\theta\right\}, \tag{A7}$$

where E^+ is the total shoreward propagating energy in the infragravity band D_f of width Δ_f.

[23] To assess the errors in equation (A7), it is convenient to normalize by the true shoreward energy flux

$$F_t^+ = \sqrt{gh}\,E^+\int_{-\pi/2}^{\pi/2} S(\theta)\cos\theta d\theta\,,$$

yielding

$$\frac{F^+}{F_t^+} = \left(1 + \beta R_t + R_0^2R_t^2\right)\frac{F_0^+}{F_t^+}\,(= 1 \text{ if } F^+ \text{ is exact}), \tag{A8}$$

$$\frac{F^-}{F_t^+} = \left(R_0^2 + \beta R_t + R_t^2\right)\frac{F_0^+}{F_t^+}\left(= R_t^2 \text{ if } F^- \text{ is exact}\right), \qquad \text{(A9)}$$

$$\frac{R^2}{R_t^2} = \frac{1 + \beta R_t^{-1} + R_t^{-2}R_0^2}{1 + \beta R_t + R_t^2 R_0^2}\left(= 1 \text{ if } R^2 \text{ is exact}\right), \qquad \text{(A10)}$$

where R_0^2 and F_0^+ are the values of the estimated reflection coefficient and shoreward flux for ${R_t}^2 = 0$ and

$$R_0^2 = \frac{a-b}{a+b},\ F_0^+ = \frac{\sqrt{gh}}{4}\ E^+(a+b), \qquad \beta = \frac{c}{a+b}, \qquad \text{(A11)}$$

with

$$a = \int_{-\pi/2}^{\pi/2} S(\theta)(1+\cos^2\theta)d\theta, \quad b = \int_{-\pi/2}^{\pi/2} 2S(\theta)\cos\theta d\theta$$
$$c = 2\Delta_f \int_{D_f} d_f \int_{-\pi/2}^{\pi/2} S(\theta)\sin(2\phi)\sin^2\theta d\theta. \qquad \text{(A12)}$$

Assuming that the beach slope is constant, the integral (A3) becomes

$$\phi(f,x,\theta) = \frac{2\pi f x}{\sqrt{gh(x)}}\left[\cos\theta + \frac{\theta}{\sin\theta}\right]. \qquad \text{(A13)}$$

[24] The errors in the estimates (A8)–(A10) can be calculated for a given ${R_t}^2$ if values of ${R_0}^2$, β and ${F_0}^+/{F_t}^+$ are known. These depend on $S(\theta)$ and are obtained by substituting in equation (A12) an analytic expression for S [*Longuet-Higgins et al.*, 1963],

$$S(\theta) = A\left[\cos(\theta - \theta_m)\right]^{2(2/\sigma^2-1)}, \qquad \text{(A14)}$$

where A is a normalization constant, θ_m is the mean propagation direction, and σ is the directional width. The dependence of R_0^2, β, and F_0^+/F_t^+ in equations (A8)–(A10) on θ_m and σ is shown in Figures A1a–A1c. The infragravity band was taken as 0.01–0.03 Hz (a wider bandwidth reduces the errors), and the beach slope was taken as 0.02 (approximately the average Duck slope over the span of the sensor array). Figure A1b shows the magnitude of the maximum of $|\beta|$ over the depth range 1–6 m. For typical observed θ_m and σ, values of $|\beta|$, R_0^2, and F_0^+/F_t^+ are about 0.005, 0.0015, and 1.1, respectively. With these values the relative errors for R^2 and $F^{\pm}$ do not exceed 20% for $0.05 < {R_t}^2 < 4$ (Figure A1d). Note that because the fluxes $F^{\pm}$ are overestimated by approximately the same amount, the flux ratio R^2 is more accurate than the fluxes

[25] **Acknowledgments.** This research was supported by the Office of Naval Research, the National Ocean Partnership Program, and the Mellon Foundation. Staff from the Center for Coastal Studies, Scripps Institution of Oceanography, and from U.S. Army Corps of Engineers Field Research Facility, Duck, North Carolina, provided excellent logistical support. Britt Raubenheimer and Falk Feddersen contributed to the experiment. The 8 m array data were provided by the Field Research Facility. Woods Hole Oceanographic Institution contribution 10453.

References

Elgar, S., and R. T. Guza, Observations of bispectra of shoaling surface gravity waves, *J. Fluid Mech.*, *161*, 425–448, 1985.

Elgar, S., T. H. C. Herbers, and R. T. Guza, Reflection of ocean surface gravity waves from a natural beach, *J. Phys. Oceanogr.*, *24*, 1503–1511, 1994.

Elgar, S., R. T. Guza, W. C. O'Reilly, B. Raubenheimer, and T. H. C. Herbers, Observations of wave energy and directions near a pier, *J. Waterw. Port Coastal Ocean Eng.*, *127*, 2–6, 2001.

Feddersen, F., R. T. Guza, S. Elgar, and T. H. C. Herbers, Velocity moments in alongshore bottom stress parameterization, *J. Geophys. Res.*, *105*, 8673–8686, 2000.

Guza, R. T., E. B. Thornton, and R. A. Holman, Swash on steep and shallow beaches, paper presented at 19th Coastal Engineering Conference, Am. Soc. of Civ. Eng., Houston, Tex., 1984.

Hasselmann, K., On the non-linear energy transfer in a gravity-wave spectrum, part 1, General theory, *J. Fluid Mech.*, *12*, 481–500, 1962.

Herbers, T. H. C., and M. C. Burton, Nonlinear shoaling of directionally spread waves on a beach, *J. Geophys. Res.*, *102*, 21,101–21,114, 1997.

Herbers, T. H. C., S. Elgar, and R. T. Guza, Infragravity frequency (0.005–0.05 Hz) motions on the shelf, part I, Forced waves, *J. Phys. Oceanogr.*, *24*, 917–927, 1994.

Herbers, T. H. C., S. Elgar, and R. T. Guza, Infragravity frequency (0.005–0.05 Hz) motions on the shelf, part II, Free waves, *J. Phys. Oceanogr.*, *25*, 1063–1079, 1995a.

Herbers, T. H. C., S. Elgar, R. T. Guza, and W. C. O'Reilly, Generation and propagation of infragravity waves, *J. Geophys. Res.*, *100*, 24,863–24,872, 1995b.

Herbers, T. H. C., S. Elgar, and R. T. Guza, Directional spreading of waves in the nearshore, *J. Geophys. Res.*, *104*, 7683–7693, 1999.

Herbers, T. H. C., S. Elgar, N. A. Sarap, and R. T. Guza, Nonlinear dispersion of surface gravity waves in shallow water, *J. Phys. Oceanogr.*, in press, 2002.

Huntley, D. A., Long-period waves on a natural beach, *J. Geophys. Res.*, *81*, 6441–6449, 1976.

Huntley, D. A., R. T. Guza, and E. B. Thornton, Field observations of surf beat, 1, Progressive edge waves, *J. Geophys. Res.*, *86*, 6451–6466, 1981.

Lippmann, T. C., R. A. Holman, and A. J. Bowen, Generation of edge waves in shallow water, *J. Geophys. Res.*, *102*, 8663–8679, 1997.

List, J. H., A model for the generation of two-dimensional surf beat, *J. Geophys. Res.*, *97*, 5623–5635, 1992.

Longuet-Higgins, M. S., and R. W. Stewart, Radiation stress and mass transport in surface gravity waves with application to "surf beats,", *J. Fluid Mech.*, *13*, 481–504, 1962.

Longuet-Higgins, M. S., D. E. Cartwright, and N. D. Smith, Observation of the directional spectrum of sea waves using the motions of a floating buoy, in *Ocean Wave Spectra*, pp. 111–136, Prentice-Hall, Old Tappan, N. J., 1963.

Meadows, G. A., R. A. Shuchman, and J. D. Lyden, Analysis of remotely sensed long-period wave motions, *J. Geophys. Res.*, *87*, 5731–5740, 1982.

Munk, W. H., Surf beat, *Eos Trans AGU*, *30*, 849–854, 1949.

Oltman-Shay, J., and P. A. Howd, Edge waves on non-planar bathymetry and alongshore currents: A model-data comparison, *J. Geophys. Res.*, *98*, 2495–2507, 1993.

Ruessink, B. G., Bound and free infragravity waves in the nearshore zone under breaking and non-breaking conditions, *J. Geophys. Res.*, *103*, 12,795–12,805, 1998.

Stoker, J. J., *Water Waves*, Wiley-Interscience, New York, 1947.

Suhayda, J. N., Standing waves on beaches, *J. Geophys. Res.*, *79*, 3065–3071, 1974.

Symonds, G., D. A. Huntley, and A. J. Bowen, Two-dimensional surf beat: Long wave generation by time varying breakpoint, *J. Geophys. Res.*, *81*, 492–498, 1982.

Wu, N., *The Maximum Entropy Method*, Springer-Verlag, New York, 1997.

S. Elgar, Woods Hole Oceanographic Institution, MS 11, Woods Hole, MA 02543, USA. (elgar@whoi.edu)

R. T. Guza, Integrative Oceanography Division, Scripps Institution of Oceanography, La Jolla, CA 92093-0209, USA. (rtg@coast.ucsd.edu)

T. H. C. Herbers, Department of Oceanography, Naval Postgraduate School, Monterey, CA 93943-5122, USA. (herbers@oc.nps.navy.mil)

A. Sheremet, Coastal Studies Institute and Department of Oceanography and Coastal Sciences, Louisiana State University, Howe-Russell Geoscience Complex, Baton Rouge, LA, 70803 USA. (ashere1@lsu.edu)